

IQNN-CS: Interpretable Quantum Neural Network for Credit Scoring

Abdul Samad Khan¹, Nouhaila Innan^{2,3}, Aeysha Khalique¹, and Muhammad Shafique^{2,3}

¹ Lahore University of Management Sciences, Pakistan

² eBRAIN Lab, Division of Engineering, New York University Abu Dhabi (NYUAD), Abu Dhabi, UAE

³ Center for Quantum and Topological Systems (CQTS), NYUAD Research Institute, NYUAD, Abu Dhabi, UAE
24120006@lums.edu.pk, nouhaila.innan@nyu.edu,
aeysha.khalique@lums.edu.pk, muhammad.shafique@nyu.edu

Abstract. Credit scoring is a high-stakes task in financial services, where model decisions directly impact individuals' access to credit and are subject to strict regulatory scrutiny. While Quantum Machine Learning (QML) offers new computational capabilities, its black-box nature poses challenges for adoption in domains that demand transparency and trust. In this work, we present IQNN-CS, an interpretable quantum neural network framework designed for multiclass credit risk classification. The architecture combines a variational QNN with a suite of post-hoc explanation techniques tailored for structured data. To address the lack of structured interpretability in QML, we introduce Inter-Class Attribution Alignment (ICAA), a novel metric that quantifies attribution divergence across predicted classes, revealing how the model distinguishes between credit risk categories. Evaluated on two real-world credit datasets, IQNN-CS demonstrates stable training dynamics, competitive predictive performance, and enhanced interpretability. Our results highlight a practical path toward transparent and accountable QML models for financial decision-making.

Keywords: Quantum Machine Learning · Credit Scoring · Interpretability · Quantum Finance

1 Introduction

Credit scoring is a foundational task in financial services, directly influencing decisions related to loan approvals, credit limits, and interest rates [1]. Its impact is not only financial but also societal, affecting individuals' access to economic opportunities. As such, credit scoring systems must meet two core requirements: high predictive performance and strict compliance with fairness and transparency regulations, such as the European Union's General Data Protection Regulation (GDPR) and the Basel III banking regulations. In this context,

interpretability becomes essential, not as an optional enhancement, but as a mandatory feature for deployment in regulated environments.

Quantum Neural Networks (QNNs) have recently emerged as promising models for structured learning tasks, owing to their potential to encode and process high-dimensional data using fewer resources [2, 3]. Their expressive power enables them to represent complex decision boundaries for domains like finance, where patterns in structured tabular data can be subtle and interdependent.

However, existing QNN-based models often prioritize performance over interpretability, which is crucial for sensitive decision-making contexts such as credit scoring. Moreover, the development of interpretable QNNs remains in its infancy. Unlike classical models, where attribution methods and explanation techniques are well-studied, the quantum learning community lacks standardized tools to reason about QNN decisions, especially in multiclass classification settings. In this work, we ask a central question:

How can QNNs be designed for real-world credit scoring applications, where achieving high accuracy is not sufficient, and interpretability is a core requirement?

To address this, we propose **IQNN-CS**, an interpretable architecture of QNNs specifically tailored for multiclass credit scoring. Our goal is not to demonstrate quantum supremacy or to outperform classical machine learning models, but rather to explore how QNNs can be made suitable for high-stakes financial applications through interpretability-aware design.

The main contributions of this paper are as follows:

- We propose a hybrid classical–quantum pipeline where a variational QNN performs classification on structured financial data, with interpretability achieved using adapted classical and quantum techniques.
- We introduce Inter-Class Attribution Alignment (ICAA), a new metric that quantifies attribution divergence across predicted classes, enabling structured analysis of model reasoning in multiclass tasks.
- We evaluate IQNN-CS on two real-world credit datasets, focusing on robustness, attribution behavior, and interpretability, while emphasizing deployment feasibility in regulated financial settings.

2 Background and Related Work

2.1 QML for Credit Scoring

Quantum Machine Learning (QML) has been increasingly applied in the financial sector [4], covering applications such as loan eligibility prediction [5], credit default classification [6], market prediction [7, 8], fraud detection [9–12], and other financial applications [13, 14]. Some of these tasks are naturally formulated as classification problems, while others are formulated as combinatorial optimization problems. Within this broad spectrum, credit scoring has received limited but growing attention in QML research.

When it comes to credit scoring, only a few works have directly addressed the problem using quantum models. The systemic quantum score model introduced a quantum kernel-based approach aimed at improving generalization in low-data and imbalanced settings, demonstrating performance benefits in a production-grade financial scenario [15]. A separate study explored a hybrid quantum–classical model for credit scoring among small- and medium-sized enterprises, highlighting reductions in training time by embedding a quantum layer into a classical neural network [16]. Both approaches treated credit scoring as a binary classification task and focused on performance rather than transparency or explainability.

Other research efforts have framed credit scoring as an optimization problem. One study utilized a QUBO formulation to optimize scoring card thresholds and combinations, employing both quantum annealing and classical heuristics to enhance bank profitability under credit risk constraints [17]. A related work investigated cost-effective feature selection for mobile credit scoring using a quantum-inspired evolutionary algorithm based on quantum gates and representations, achieving reduced feature costs and competitive accuracy [18].

While these studies highlight the potential of quantum and quantum-inspired models for credit scoring, they either treat the task as binary classification or focus on optimization formulations. Crucially, they overlook the interpretability requirements critical for real-world deployment in regulated financial environments. In contrast, we address credit scoring as a multiclass classification problem and focus on the interpretability of quantum models, an aspect that has not been covered in prior work.

2.2 Interpretability in QML

Interpretability in QML is increasingly important for deploying models in sensitive domains such as finance. However, most classical explainability methods do not directly extend to quantum models due to their probabilistic nature and circuit-based representations.

Initial efforts, such as Q-LIME, adapt local explanation techniques to quantum settings by approximating the influence of features on predictions [19]. Other works combine quantum autoencoders with classifiers and apply LIME and SHAP for interpretability in quantum representation learning [20].

To address global explainability, frameworks like QuXAI use Q-MEDLEY to trace feature attributions through quantum feature maps [21]. Visual tools such as QGrad-CAM further enable fine-grained class-specific explanations using variational quantum circuits [22]. Despite these advances, interpretability for structured, multiclass QML tasks, such as credit scoring, remains largely unexplored. Our work addresses this gap through a domain-specific, interpretable QNN framework.

3 Methodology

The IQNN-CS framework is structured as a five-stage pipeline designed to deliver interpretable and accurate credit scoring using a hybrid quantum-classical architecture (see Fig. 1 and Appendix Algorithm 1).

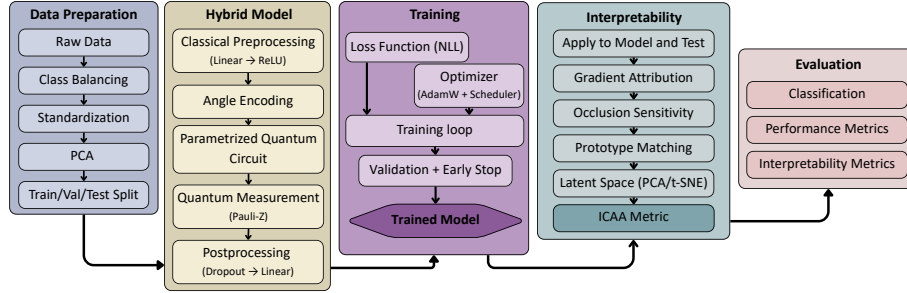


Fig. 1. Overview of the IQNN-CS pipeline.

3.1 Data Preparation

The process begins with preprocessing two benchmark credit datasets containing numerical and categorical financial attributes. To address class imbalance, we apply undersampling to Dataset 1 and SMOTE to Dataset 2, depending on the severity of imbalance. All numerical features are standardized by transforming each feature x_j to $x'_j = (x_j - \mu_j)/\sigma_j$, where μ_j and σ_j denote the empirical mean and standard deviation. To reduce dimensionality and ensure compatibility with quantum hardware constraints, Principal Component Analysis (PCA) is applied, resulting in quantum-compatible input vectors. PCA projects the data \mathbf{x} onto a lower-dimensional subspace using orthogonal components \mathbf{w}_k as $z_k = \mathbf{w}_k^\top \mathbf{x}$, for $k = 1, \dots, d$. The resulting representation aligns with the available number of qubits. Stratified sampling is used to divide the dataset into training, validation, and test sets, preserving class distribution.

3.2 Hybrid Quantum-Classical Model

The model architecture consists of three sequential components. First, a classical preprocessing block transforms the PCA-compressed input $\mathbf{z} \in \mathbb{R}^d$ into an encoded latent vector $\mathbf{h}_{cl1} \in \mathbb{R}^{d'}$ through fully connected layers with ReLU activations. This output \mathbf{h}_{cl1} is then passed to the quantum layer, where the features are encoded onto N_Q qubits, typically initialized to the $|0\rangle^{\otimes N_Q}$ state, using angle encoding, where each input feature ϕ_j (from \mathbf{h}_{cl1}) rotates a qubit via an operation like $R_P(\phi_j) = e^{-i\phi_j P/2}$, with P being a Pauli operator (e.g., $\sigma_x, \sigma_y, \sigma_z$). This is followed by a multi-layer entangling variational quantum circuit (VQC), $U(\theta)$, parameterized by trainable angles θ . Expectation values of Pauli-Z observables, $\langle \sigma_z^{(k)} \rangle = \langle \psi_0 | U^\dagger(\theta) \sigma_z^{(k)} U(\theta) | \psi_0 \rangle$ for each qubit k , are measured to extract quantum features. These features are concatenated and forwarded to the classical postprocessing head. This final block, which includes dropout regularization and linear projections, produces logits $\mathbf{o} \in \mathbb{R}^C$ over the C credit risk classes. The full system is end-to-end differentiable and implemented via Pen-

nyLane’s `TorchLayer`, enabling seamless integration with PyTorch’s automatic differentiation capabilities.

3.3 Training Procedure

The model is trained using the negative log-likelihood (NLL) loss function, given for a batch of M samples as $L_{NLL} = -\frac{1}{M} \sum_{i=1}^M \sum_{c=1}^C y_{i,c} \log(\hat{y}_{i,c})$, where $y_{i,c}$ is the ground-truth indicator for class c and $\hat{y}_{i,c}$ is the predicted probability from the softmax output. Optimization is performed with AdamW, which introduces decoupled weight decay. Learning rate scheduling, such as cosine annealing, is employed to stabilize convergence. Quantum gradients with respect to variational parameters θ are computed using the parameter-shift rule: $\frac{\partial \langle \hat{O} \rangle}{\partial \theta_k} = \frac{1}{2s} \left(\langle \hat{O} \rangle_{\theta_k+s} - \langle \hat{O} \rangle_{\theta_k-s} \right)$, with $s = \pi/2$ for single-qubit gates. Early stopping is applied based on validation loss to prevent overfitting, and the best-performing model checkpoint is retained.

3.4 Post-Hoc Interpretability

Interpretability is assessed using four complementary techniques (see Appendix Algorithm 2). First, gradient-based attribution methods, including saliency maps, gradient×input, integrated gradients, and SmoothGrad, estimate the importance of each input feature x_j through $\partial L / \partial x_j$ or related formulations. Second, prototype matching is performed in the quantum feature space by extracting activation vectors $\mathbf{a}_{QNN}(x)$ and computing cosine similarity with training instances: $S_C(\mathbf{u}, \mathbf{v}) = \frac{\mathbf{u} \cdot \mathbf{v}}{\|\mathbf{u}\| \|\mathbf{v}\|}$. This allows retrieval of similar historical examples for a given test input. Fourth, we introduce the ICAA metric. For each class c , let $\mathbf{A}_c(x_{inst})$ be its attribution vector. The ICAA matrix is defined by: $ICAA_{ij}(x_{inst}) = S_C(\mathbf{A}_i(x_{inst}), \mathbf{A}_j(x_{inst}))$, capturing the pairwise similarity in feature attributions across classes. Additionally, we assess the region of indecision by perturbing inputs and measuring the variance in attribution vectors.

3.5 Evaluation Metrics

The final model performance is evaluated using accuracy and macro F1-score. Accuracy is computed as $\text{Acc} = \frac{TP+TN}{TP+TN+FP+FN}$, where TP is the number of true positives, TN is the number of true negatives, FP is the number of false positives, and FN is the number of false negatives. while the macro F1-score aggregates class-wise F1-scores: $F1_c = \frac{2P_c R_c}{P_c + R_c}$, $\text{Macro F1} = \frac{1}{C} \sum_{c=1}^C F1_c$, where P_c and R_c are precision and recall for class c . Confusion matrices offer class-level diagnostic insights. Finally, we visualize interpretability outputs, gradient maps, and matched prototypes, along with latent space projections of QNN activations using t-SNE. These projections are color-coded by true labels to assess the separability of quantum features.

4 Results

4.1 Experimental Settings

Experiments were conducted on two benchmark credit scoring datasets: Dataset 1 [23] and Dataset 2 [24]. All models were implemented using PyTorch and

PennyLane [25], with quantum circuits simulated via `default.qubit`. Training was executed on a CPU (Apple M3, 16 GB RAM) without GPU acceleration. Each dataset was split into training (70%), validation (15%), and test (15%) sets using stratified sampling. The hybrid model combined six qubits and four `StronglyEntanglingLayers` with classical dense layers and dropout. Optimization was performed over 50 epochs using the AdamW optimizer (learning rate 0.01) and class-weighted cross-entropy loss. Full configuration details are provided in Appendix Table 2.

4.2 Training and Convergence

Fig. 2 shows the training, validation, and test curves for both datasets. For Dataset 1, accuracy curves in (a) exhibit rapid improvement within the first few epochs, stabilizing above 98% across all splits. The corresponding loss curves in (b) show a sharp decrease followed by a smooth plateau, with minimal discrepancy between training and validation, indicating efficient convergence and strong generalization. In contrast, Dataset 2 exhibits more unstable training behavior.

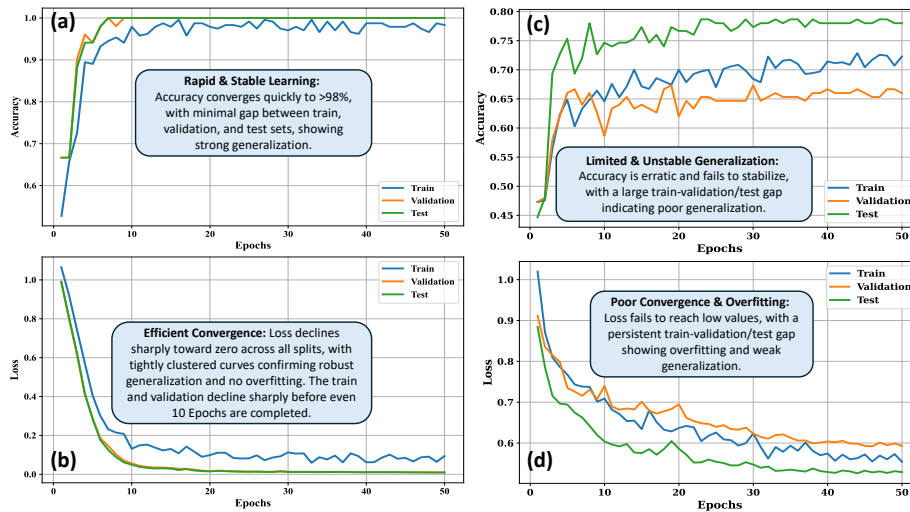


Fig. 2. Accuracy and loss curves for IQNN-CS. (a) accuracy and (b) loss for Dataset 1; (c) accuracy and (d) loss for Dataset 2.

Accuracy trends in (c) plateau early, with validation and test performance remaining below 80%. The loss curves in (d) reveal a slower and noisier decline, particularly in the validation set. The wider gap between training and validation suggests either overfitting or greater dataset complexity due to feature diversity and class imbalance.

4.3 Classification Performance

Table 1 summarizes the classification results for both datasets. On Dataset 1, the model achieved perfect performance, with 100% accuracy and F1-score. This

confirms the model’s ability to separate risk levels cleanly in well-structured data. For Dataset 2, overall accuracy was 77.3%, with variable class-wise metrics. The model showed high recall for the Low class (0.97) but low precision (0.64), suggesting misclassifications. The High class had strong precision (0.95) but lower recall (0.67), reflecting under-identification of high-risk cases. These results highlight Dataset 2’s complexity and imbalance.

Table 1. Classification performance on both Datasets.

Class	Dataset 1			Dataset 2		
	Precision	Recall	F1-score	Precision	Recall	F1-score
Low	1.00	1.00	1.00	0.64	0.97	0.77
Average	1.00	1.00	1.00	0.73	0.84	0.78
High	1.00	1.00	1.00	0.95	0.67	0.79
Accuracy (%)	100			77.3		

4.4 Interpretability Analysis

To assess the transparency and trustworthiness of the IQNN-CS model, we conduct a comprehensive interpretability analysis. This includes examining latent quantum geometry, attribution consistency, example influence, class attribution alignment, and softmax entropy behavior. We compare findings across both datasets to understand how dataset quality impacts interpretability.

Feature Attribution Analysis: As illustrated in Fig. 3, saliency maps for a representative test instance show focused and interpretable patterns in Dataset 1. In contrast, Dataset 2 exhibits diffuse, noisy attributions that vary across runs, suggesting that the model relies less consistently on meaningful input features.

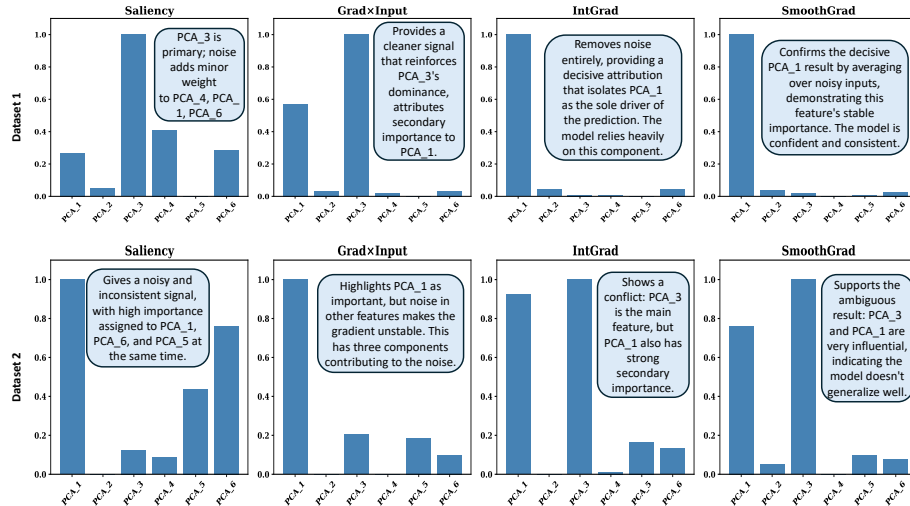


Fig. 3. Saliency maps for a selected test sample. Dataset 1 shows concentrated attributions; Dataset 2 appears more diffuse.

Quantum Representation Geometry: Latent embeddings extracted from the quantum layer are visualized using t-SNE as shown in Fig. 4. Dataset 1 shows well-separated manifolds, indicating robust internal representations. In contrast, Dataset 2 presents entangled clusters, particularly between the Average and High classes, reflecting the model’s confusion in classification.

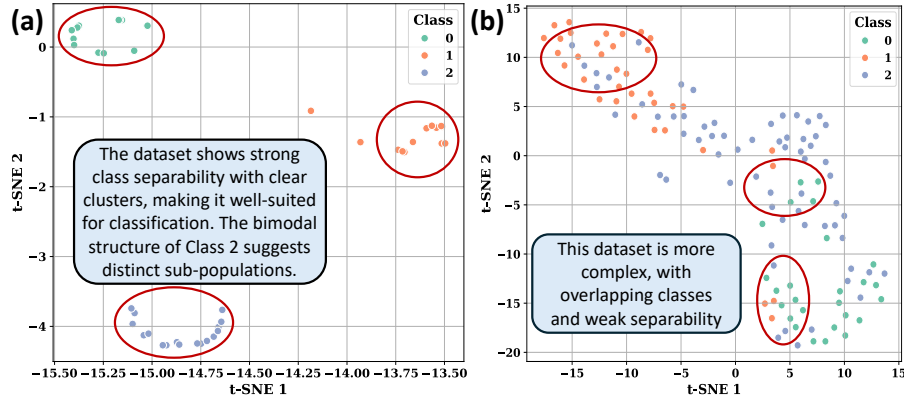


Fig. 4. t-SNE projection of quantum embeddings. (a) Dataset 1 yields a clear separation; (b) Dataset 2 shows an overlap.

Attribution Sensitivity: To assess how strongly predictions depend on top-ranked features, we occlude inputs and track confidence degradation. As shown in Fig. 5, Dataset 1 experiences sharp confidence drops, indicating reliance on a few informative features. In Dataset 2, degradation is gradual and less structured.

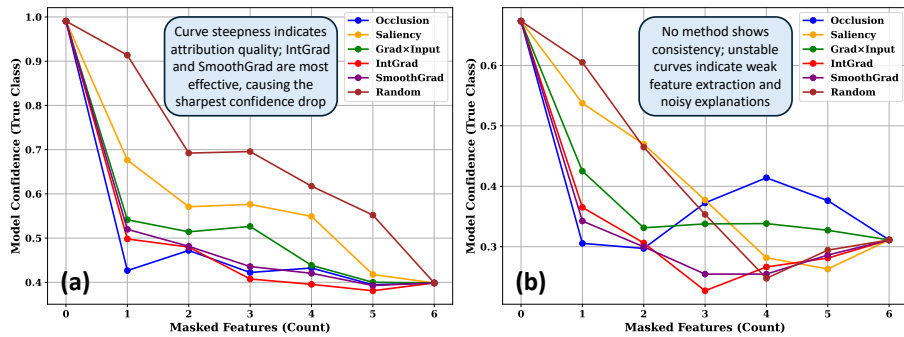


Fig. 5. Prediction confidence vs. occluded features. Left: Dataset 1 shows sharp drops; Right: Dataset 2 decays smoothly.

ICAA: We assess whether the model produces disentangled explanations for each class using ICAA. As shown in Fig. 6, Dataset 1 yields low inter-class attribution similarity, while Dataset 2 exhibits significant overlap, revealing a less distinct decision rationale.

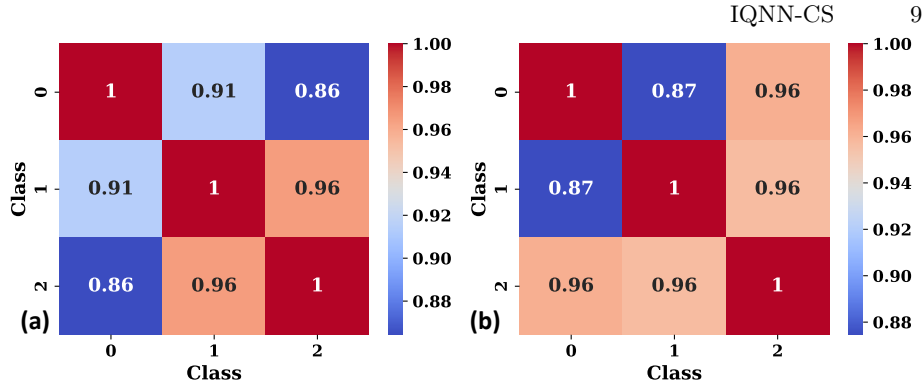


Fig. 6. ICAA matrices. Dataset 1 (a) shows clean class-wise separation; Dataset 2 (b) reveals overlapping attribution logic.

4.5 Discussion

Our experiments highlight a stark contrast in how the IQNN-CS model performs across two credit scoring datasets. While Dataset 2 proved more challenging, despite using the same model, its lower accuracy and less structured latent space suggest that the success of QNNs strongly depends on how well the data aligns with the model’s inductive bias. Dataset 2 presented complex and overlapping feature spaces that the model struggled to disentangle. Interpretability tools helped uncover these differences. Occlusion and our proposed ICAA metric revealed that, in Dataset 2, attribution patterns overlapped, indicating that the model relied on similar features across classes, a potential source of misclassification. Gradient-based explanations were inconsistent, especially in noisy predictions, suggesting they should be used cautiously in quantum settings. Additionally, example-based attribution showed that Dataset 2 often aligned with incorrect classes, despite high-confidence predictions. This shows that a model’s internal logic can break down even when output probabilities appear reliable.

In summary, these findings underscore that interpretability is not simply about explanation; it is a crucial diagnostic tool. Metrics like ICAA provide deeper insight into how well a model separates reasoning across classes, which is particularly important in high-stakes domains like finance.

5 Conclusion

We introduced IQNN-CS, a hybrid quantum-classical model for credit scoring that combines strong predictive performance with interpretable outputs. Across two real-world datasets, the model demonstrated high accuracy when the data structure aligned with its quantum encoding and revealed clear decision patterns through interpretability analysis. A key contribution of this work is the ICAA metric, which quantifies how distinctly the model reasons about different classes. It proved useful for identifying when the model’s internal logic breaks down, even when standard metrics suggest good performance. Together with attribution sensitivity and example-based influence tracing, ICAA strengthens the tools available for understanding quantum models. IQNN-CS shows that accurate quantum models can also be transparent and trustworthy. As quantum

computing advances, such interpretability-first frameworks will be essential for deploying reliable AI in sensitive fields like finance and healthcare.

Acknowledgments

This work was supported in part by the NYUAD Center for Quantum and Topological Systems (CQTS), funded by Tamkeen under the NYUAD Research Institute grant CG008, and the Center for Cyber Security (CCS), funded by Tamkeen under the NYUAD Research Institute Award G1104.

References

1. L. Thomas *et al.*, *Credit scoring and its applications*. SIAM, 2017.
2. A. Abbas *et al.*, “The power of quantum neural networks,” *Nature Computational Science*, 2021.
3. N. Innan *et al.*, “Next-generation quantum neural networks: Enhancing efficiency, security, and privacy,” in *2025 IEEE 31st International Symposium on On-Line Testing and Robust System Design (IOLTS)*, pp. 1–4, IEEE, 2025.
4. J. Biamonte *et al.*, “Quantum machine learning,” *Nature*, 2017.
5. N. Innan *et al.*, “Lep-qnn: Loan eligibility prediction using quantum neural networks,” *arXiv preprint arXiv:2412.03158*, 2024.
6. A. Sengar *et al.*, “A comparative analysis of hybrid quantum neural networks in binary credit defaulting tasks,” in *2023 IEEE MIT Undergraduate Research Technology Conference (URTC)*, IEEE, 2023.
7. P. K. Choudhary *et al.*, “Hqnn-fsp: A hybrid classical-quantum neural network for regression-based financial stock market prediction,” *arXiv preprint arXiv:2503.15403*, 2025.
8. P. Pathak, V. Oad, A. Prajapati, and N. Innan, “Resource allocation optimization in 5g networks using variational quantum regressor,” in *2024 International Conference on QCNC*, pp. 101–105, IEEE, 2024.
9. N. Innan *et al.*, “Financial fraud detection: a comparative study of quantum machine learning models,” *International Journal of Quantum Information*, 2024.
10. N. Innan *et al.*, “Qfnn-ffd: Quantum federated neural network for financial fraud detection,” in *2025 IEEE International Conference on QSW*, pp. 41–47, IEEE, 2025.
11. N. Innan *et al.*, “Financial fraud detection using quantum graph neural networks,” *Quantum Machine Intelligence*, vol. 6, no. 1, p. 7, 2024.
12. M. E. Alami *et al.*, “Comparative performance analysis of quantum machine learning architectures for credit card fraud detection,” *arXiv preprint arXiv:2412.19441*, 2024.
13. M. Kashif *et al.*, “Evaluating quantum amplitude estimation for pricing multi-asset basket options,” *arXiv preprint arXiv:2509.09432*, 2025.
14. N. Innan *et al.*, “Quantum portfolio optimization with expert analysis evaluation,” *arXiv preprint arXiv:2507.20532*, 2025.
15. J. Mancilla *et al.*, “Empowering credit scoring systems with quantum-enhanced machine learning,” *arXiv preprint arXiv:2404.00015*, 2024.
16. N. Schetakis *et al.*, “Quantum machine learning for credit scoring,” *Mathematics*, vol. 12, no. 9, p. 1391, 2024.
17. B. Zhang *et al.*, “Credit scoring card combination optimization model based on qubo,” in *Proceedings of the International Conference on Machine Learning, Pattern Recognition and Automation Engineering*, 2024.
18. C. M. Chen *et al.*, “Quantum optimized cost based feature selection and credit scoring for mobile micro-financing,” *Computational Economics*, 2024.
19. L. Pira and C. Ferrie, “On the interpretability of quantum neural networks,” *Quantum Machine Intelligence*, vol. 6, no. 2, p. 52, 2024.
20. A. Kottahachchi K.D and I. Khalil, “Qrlaxai: quantum representation learning and explainable ai,” *Quantum Machine Intelligence*, 2025.
21. S. Barua *et al.*, “Quxai: Explainers for hybrid quantum machine learning models,” *arXiv preprint arXiv:2505.10167*, 2025.
22. H.-Y. Lin *et al.*, “Quantum gradient class activation map for model interpretability,” in *2024 IEEE Workshop on SiPS*, pp. 165–170, IEEE, 2024.
23. “Credit score classification dataset.” <https://www.kaggle.com/datasets/sujithmandala/credit-score-classification-dataset>.
24. “Credit score classification dataset.” <https://www.kaggle.com/datasets/parisrohan/credit-score-classification>.
25. V. Bergholm *et al.*, “PennyLane: Automatic differentiation of hybrid quantum-classical computations,” *arXiv preprint arXiv:1811.04968*, 2018.

Appendix

A1 IQNN-CS Training Procedure

The IQNN-CS architecture is trained using a hybrid quantum-classical pipeline as detailed in Algorithm 1.

Algorithm 1 IQNN-CS Training Procedure

Require: Raw Datasets (D_{raw1}, D_{raw2}), NumEpochs (N_{epochs}), BatchSize (B), LearningRate (η), PCA Dimensions (d_{PCA1}, d_{PCA2}), Qubit Counts (N_{Q1}, N_{Q2})

Ensure: Trained IQNN-CS model ($M_{IQNN-CS}$)

- 1: Initialize the IQNN-CS model structure ($M_{IQNN-CS}$):
- 2: Define classical pre-processing network $M_{classical_pre}$ using d_{PCA} input dimensions.
- 3: Define Quantum Neural Network M_{QNN} with N_Q qubits, specified layers, and encoding method.
- 4: Define classical post-processing network $M_{classical_post}$ for the specified number of output classes.
- 5: Assemble $M_{IQNN-CS}$ by sequentially connecting $M_{classical_pre} \rightarrow M_{QNN} \rightarrow M_{classical_post}$.
- 6: **for all** dataset D_{raw} in $\{D_{raw1}, D_{raw2}\}$ **do**
- 7: \triangleright Configure dataset-specific parameters: d_{PCA}, N_Q
- 8: Perform preprocessing on D_{raw} to obtain D_{proc} :
- 9: Apply class balancing technique (e.g., Undersampling, SMOTE).
- 10: Apply feature standardization (e.g., StandardScaler).
- 11: Apply PCA to reduce dimensionality to d_{PCA} .
- 12: Split D_{proc} into training D_{train} , validation D_{val} , and test D_{test} sets.
- 13: Initialize optimizer (e.g., AdamW) with $M_{IQNN-CS}$ parameters and learning rate η .
- 14: Initialize learning rate scheduler (e.g., StepLR or CosineAnnealingLR).
- 15: **for** $epoch = 1 \rightarrow N_{epochs}$ **do**
- 16: Set $M_{IQNN-CS}$ to training mode.
- 17: **for all** batch (X_b, y_b) in D_{train} **do**
- 18: Clear gradients in the optimizer.
- 19: Obtain predictions \hat{y}_b via a forward pass of X_b through $M_{IQNN-CS}$.
- 20: Calculate loss (e.g., Negative Log-Likelihood) between \hat{y}_b and y_b .
- 21: Compute gradients via hybrid backpropagation through $M_{IQNN-CS}$.
- 22: Update model parameters using the optimizer.
- 23: **end for**
- 24: Adjust learning rate using the LR scheduler.
- 25: Set $M_{IQNN-CS}$ to evaluation mode.
- 26: Calculate validation loss $loss_{val}$ on D_{val} using $M_{IQNN-CS}$.
- 27: **if** validation loss $loss_{val}$ meets early stopping criteria **then**
- 28: **break** \triangleright Cease training if validation performance degrades or stagnates
- 29: **end if**
- 30: **end for**
- 31: **end for**
- 32: **return** Trained $M_{IQNN-CS}$

A2 Interpretability Pipeline

The interpretability module, summarized in Algorithm 2, combines gradient-based saliency maps, occlusion analysis, example-based attribution, ICAA, and latent space visualization. These methods are executed on selected test instances, allowing insight into feature influence and consistency across representations.

A3 Experimental Settings

The experimental configuration used across datasets is outlined in Table 2. This setup ensures consistency for reproducibility and fair interpretability comparisons.

A4 Extended Interpretability Analysis

Attribution Stability and Regions of Indecision: To assess robustness, we introduced Gaussian noise and computed the standard deviation of saliency

maps. Most samples showed stable attribution under perturbation. However, Sample 12 in Dataset 2 showed significantly higher variance (Table 3), indicating unreliable class evidence.

Algorithm 2 Post-hoc Interpretability Analysis

Require: Trained IQNN-CS model ($M_{IQNN-CS}$), Preprocessed Test Data (D_{test}), Set of test instances ($X_{interpret} \subseteq D_{test}$)

Ensure: Interpretability outputs (Attribution Maps, ICAA Matrix, Plots, etc.)

- 1: Set $M_{IQNN-CS}$ to evaluation mode.
- 2: **for all** test instance x_{inst} in $X_{interpret}$ **do**
- 3: ▷ 1. Gradient-Based Attribution
- 4: For each target class c :
- 5: Compute gradient-based attribution $A_c(x_{inst})$ for x_{inst} towards class c using $M_{IQNN-CS}$.
- 6: Store or visualize $A_c(x_{inst})$ (e.g., as feature heatmaps).
- 7: ▷ 2. Occlusion Analysis
- 8: Perform occlusion analysis on x_{inst} with $M_{IQNN-CS}$ to obtain prediction probability drop curve P_{drop_curve} .
- 9: ▷ This involves iteratively masking features of x_{inst} and recording the drop in prediction probability.
- 10: Store or visualize P_{drop_curve} .
- 11: ▷ 3. Example-Based Attribution (using QNN Activations)
- 12: **if** QNN activations for training data are not precomputed **then**
- 13: Extract QNN activations Act_{train} from M_{QNN} for all instances in D_{train} .
- 14: **end if**
- 15: Extract QNN activation act_{inst} from M_{QNN} for instance x_{inst} .
- 16: Calculate cosine similarity scores Sim_{scores} between act_{inst} and all activations in Act_{train} .
- 17: Identify influential training examples based on Sim_{scores} .
- 18: ▷ 4. Inter-Class Attribution Alignment (ICAA)
- 19: Let $A_0(x_{inst}), A_1(x_{inst}), \dots$ be the attribution vectors for x_{inst} for each class (obtained from gradient-based attribution).
- 20: Calculate $ICAA_{ij} \leftarrow \text{CosineSimilarity}(A_i(x_{inst}), A_j(x_{inst}))$ for all pairs of classes (i, j) .
- 21: Store the resulting $ICAA_{matrix}$ for x_{inst} .
- 22: **end for**
- 23: ▷ 5. Latent Space Geometry Visualization (on a subset of D_{test})
- 24: Select a subset X_{subset} from D_{test} .
- 25: Extract QNN activations Act_{QNN_subset} from M_{QNN} for all instances in X_{subset} .
- 26: Apply a dimensionality reduction technique (e.g., t-SNE or PCA) to Act_{QNN_subset} .
- 27: Plot the reduced-dimension embeddings, coloring them by true class labels.
- 28: **return** All generated interpretability maps, matrices, plots, and insights.

Table 2. Experimental Configuration for IQNN-CS

Component	Setting
Quantum Framework	PennyLane (default.qubit)
Number of Qubits	6
Quantum Layers	4 (StronglyEntanglingLayers)
Embedding Strategy	AngleEmbedding
Classical Layers	Linear \rightarrow ReLU \rightarrow Linear + Dropout
Preprocessing	StandardScaler, OneHotEncoder, SMOTE
Dimensionality Reduction	PCA (6 components)
Batch Size	16
Optimizer	AdamW
Learning Rate	0.01
Scheduler	StepLR
Loss Function	CrossEntropy (class-weighted)
Epochs	50
Validation Strategy	70-15-15 train-val-test split (stratified)
Random Seed	42 (NumPy + PyTorch)

Table 3. Standard deviation of saliency maps under 20 random Gaussian perturbations for selected test samples.

Sample	Dataset 1 (std)	Dataset 2 (std)	Indecisive?
3	0.0493	0.0651	No
7	0.1570	0.0395	No
12	0.1426	0.2797	Yes

Influence of Training Examples on Test Samples: We analyze the influence of training samples on test instance 7 using test-to-train cosine similarity. As shown in Table 4, in Dataset 1, the most influential samples align with the test sample’s true class, indicating coherent internal representations. In contrast, Dataset 2 shows high-similarity points from multiple classes, suggesting ambiguity in the learned decision boundary.

Table 4. Cosine similarity between test sample 7 and top influential training examples in both datasets. Dataset 1 shows high similarity to same-class examples, while Dataset 2 yields a mix of same and different-class influences, suggesting less coherent internal representations.

Dataset	Test Sample	Train Index	Label	Cosine Sim.	Observation
1	7	146	2	0.9989	Same class as test
1	7	181	2	0.9976	Same class as test
1	7	160	2	0.9976	Same class as test
1	7	22	2	0.9930	Same class as test
1	7	94	2	0.9416	Same class as test
2	7	503	1	1.0000	Different class
2	7	19	1	1.0000	Different class
2	7	433	1	1.0000	Different class
2	7	588	1	1.0000	Different class
2	7	173	2	1.0000	Same class as test

Prediction Confidence and Attribution Consistency Fig. 7 shows that Dataset 1 had sharper softmax distributions, indicating high-confidence predictions. Dataset 2 yielded broader distributions, consistent with noisy convergence and less reliable model explanations. While the attribution similarity matrix (Fig. 8) reveals well-separated patterns in Dataset 1, while Dataset 2 lacks structure, underscoring inconsistency in explanation reliability.

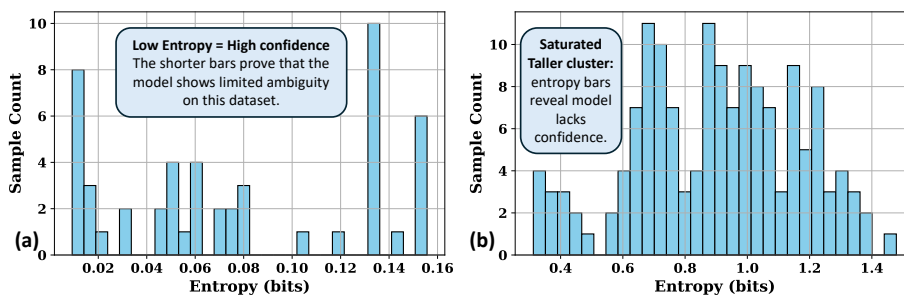


Fig. 7. Softmax entropy distributions. Dataset 1 (a) exhibits lower uncertainty compared to Dataset 2 (b).

Method Evaluation Summary: Table 5 synthesizes the comparative effectiveness of various interpretability techniques across both datasets. The evaluation is based on how well each method provides meaningful, class-consistent, and stable explanations aligned with model behavior.

In Dataset 1, most interpretability methods yielded coherent and high-confidence outputs. Occlusion and ICAA emerged as the most reliable techniques, offering sharply localized and class-discriminative explanations. Gradient-based methods such as saliency maps and integrated gradients also performed well, whereas SmoothGrad shows limited value due to noise sensitivity. In Dataset 2, the utility

of nearly all methods degraded, consistent with earlier findings of unstable training dynamics and less confident predictions. ICAA and occlusion retained partial utility but suffered from reduced clarity. Example-based attributions revealed inconsistencies in training-test relationships, and attribution stability flagged specific instances of model indecision. Overall, the summary table highlights that interpretability reliability is closely tied to training convergence quality and dataset structure. Robust interpretability requires not only method design but also stable and semantically meaningful latent representations from the model itself.

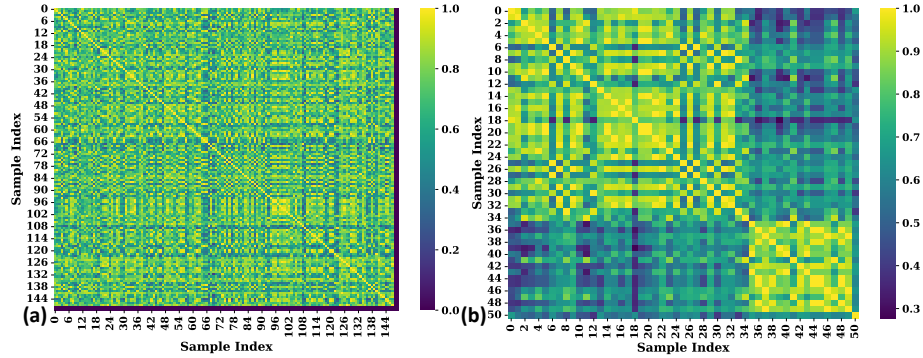


Fig. 8. Attribution similarity matrices across test samples for both Datasets: Dataset 1 (a) and Dataset 2 (b).

Table 5. Interpretability method utility across both datasets.

Method	Dataset 1 Utility	Dataset 2 Utility
Saliency	High	Medium
Gradient \times Input	Moderate	Low
Integrated Gradients	High	Medium
SmoothGrad	Low	Low
Occlusion	Very High	Medium
ICAA	Very High	Medium
Example-Based	High	Low
Indecision Detection	Clean (all stable)	Useful (flagged Sample 12)